Journal of the Meteorological Society of Japan, Vol. 73, No. 2B, pp. 443–459, 1995

Doppler Radar Observations on the Structure and Characteristics of Tropical Clouds during TOGA-COARE IOP in Manus, Papua New Guinea: Dual-Doppler Analysis of Mesoscale Convective Systems Composing a Cloud Cluster

By Shinsuke Satoh

Institute of Low Temperature Science, Hokkaido University, Sapporo 060, Japan

Atsushi Kinoshita[1] and Hiroshi Uyeda

Department of Geophysics, Faculty of Science, Hokkaido University, Sapporo 060, Japan

(Manuscript received 4 July 1994, in revised form 19 January 1995)

Abstract

Three distinct mesoscale convective systems (MCSs), composing a tropical cloud cluster, observed on January 18–19, 1993 were investigated. This event was observed by two Doppler radars on Manus Island (2°S, 147°E), Papua New Guinea, during the TOGA-COARE IOP. The cloud cluster was formed within the radar range, and extended to a diameter of about 200 km. The environmental wind was weak, but a strong vertical shear existed at the middle level (3–8 km).

The first characteristic MCS moved faster than the environmental wind, and thus is referred to as a fast-moving convective system (FMCS). The orientation of this FMCS was nearly perpendicular to the direction of the dominant vertical shear. Behind the convective cell of the FMCS, an anvil echo extended to upper levels. The front inflow had two branching sub-flows in front of the convective cell with a strong downdraft. The lower level outflow from the downdraft also branched out to southward and northward flows. The branching inflow and outflow were associated with symmetrically-arranged strong convergence regions. These features were similar to a structure produced by the storm splitting, and is recognized as a squall line system with a three-dimensional structure. The second MCS was composed of individual convective cells, moving at a slower speed than the first system. This slow-moving convective system (SMCS) was associated with the south-easterly inflow at lower levels, and extended in a line parallel to the vertical shear direction from north to south. The last system was a stratiform-looking echo system marked by an obvious bright band at the melting level. This system brought more precipitation than the other MCSs. In the echo system, a vortex with a diameter of 20 km was found at the middle layer (4–6 km). In the middle layer, some vertical circulations were also found, and vertical circulations with a maximum velocity of 5 m s^{-1} were found in the upper layer (> 6 km). These circulations seemed to cause the heavy precipitation.

1. Introduction

It has been recognized that a cloud cluster is composed of several mesoscale convective systems (MCSs), whose structure has been studied for various regions (Houze, 1977; Zipser, 1977; Leary and Houze, 1979a; Ishihara, 1985; Smull and Houze, 1987; Akaeda *et al.*, 1991; Mori, 1992; Keenan and Rutledge, 1993).

In the tropics, cloud clusters and MCSs were studied mainly through several comprehensive field experiments, such as the Global Atmospheric Research Program's Atlantic Tropical Experiment (GATE) in 1974. Although it is difficult to classify the shapes of the MCSs, it has been known that a line-shaped system occurs frequently. Houze and Betts (1981) summarized convective systems observed in GATE, and characterized line-shaped MCSs as a squall line

1 Present affiliation: Bekkai High School, Bekkai, Hokkaido, Japan.

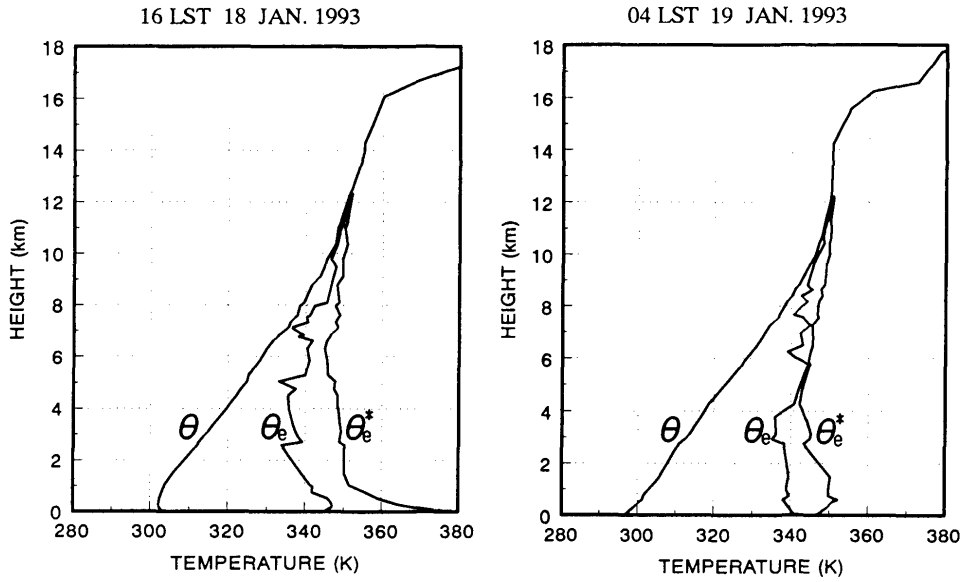

Fig. 1. Vertical profiles of potential temperature θ, equivalent potential temperature θe and saturation equivalent potential temperature θe^* deduced from soundings at Manus before (1600 LST on 18) and after (0400 LST on 19) the cloud cluster development.

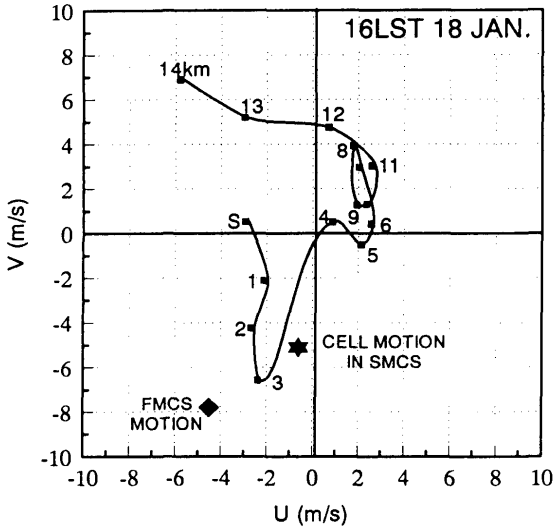

Fig. 2. Wind hodograph before (1600 LST) the cloud cluster development deduced from a rawinsonde. Numbers are heights in kilometers above mean sea level.

and a non-squall line from the data. Barnes and Sieckman (1984) classified MCSs into fast- and slow-moving cloud systems. The fast-moving cloud line is synonymous with a squall line, and the slow-moving cloud line is synonymous with a non-squall line. They showed that the orientation of the fast-moving cloud line was normal to the environmental vertical shear of the lower layer (< 650 hPa), whereas that of the slow-moving cloud line was parallel to the vertical shear. They also showed that the fast-moving lines had a more-dry layer at the middle level.

Based on the observations from the Convection Profonde Tropicale (COPT 81) experiment in western Africa with a dual-Doppler radar system, Chong *et al.* (1987) studied the three-dimensional airflow structure of a tropical squall line, and Roux (1988) examined the kinematics and thermodynamics of the convective region in a squall line.

In the past, more studies focused on squall lines with a well-defined structure and a fast propagation, despite of their fewer occurrences than other MCSs. Furthermore, the MCSs with squall lines of the Atlantic ocean were influenced by the African wave (Chen, 1985).

Even though the western tropical Pacific ocean with high temperature is the most important for a forcing of global atmospheric circulation, there have been very few experiments before the Tropical Ocean Global-Atmosphere program, Coupled Ocean-Atmosphere Response Experiment (TOGA-COARE) over the western tropical Pacific ocean from November 1992 to January 1993 as the Intensive Observation Period (IOP).

The purpose of this study is to describe the three-dimensional kinematic structures of MCSs, composing a tropical cloud cluster, observed on January 18–19, 1993. This event was observed by a dual-Doppler radar system on Manus Island (2°S, 147°E), Papua New Guinea, during the TOGA-COARE IOP.

2. Data and method of analysis

Data used in this study were acquired with two X-band Doppler radars of the Institute of Low Temperature Science (ILTS) and Hokkaido University

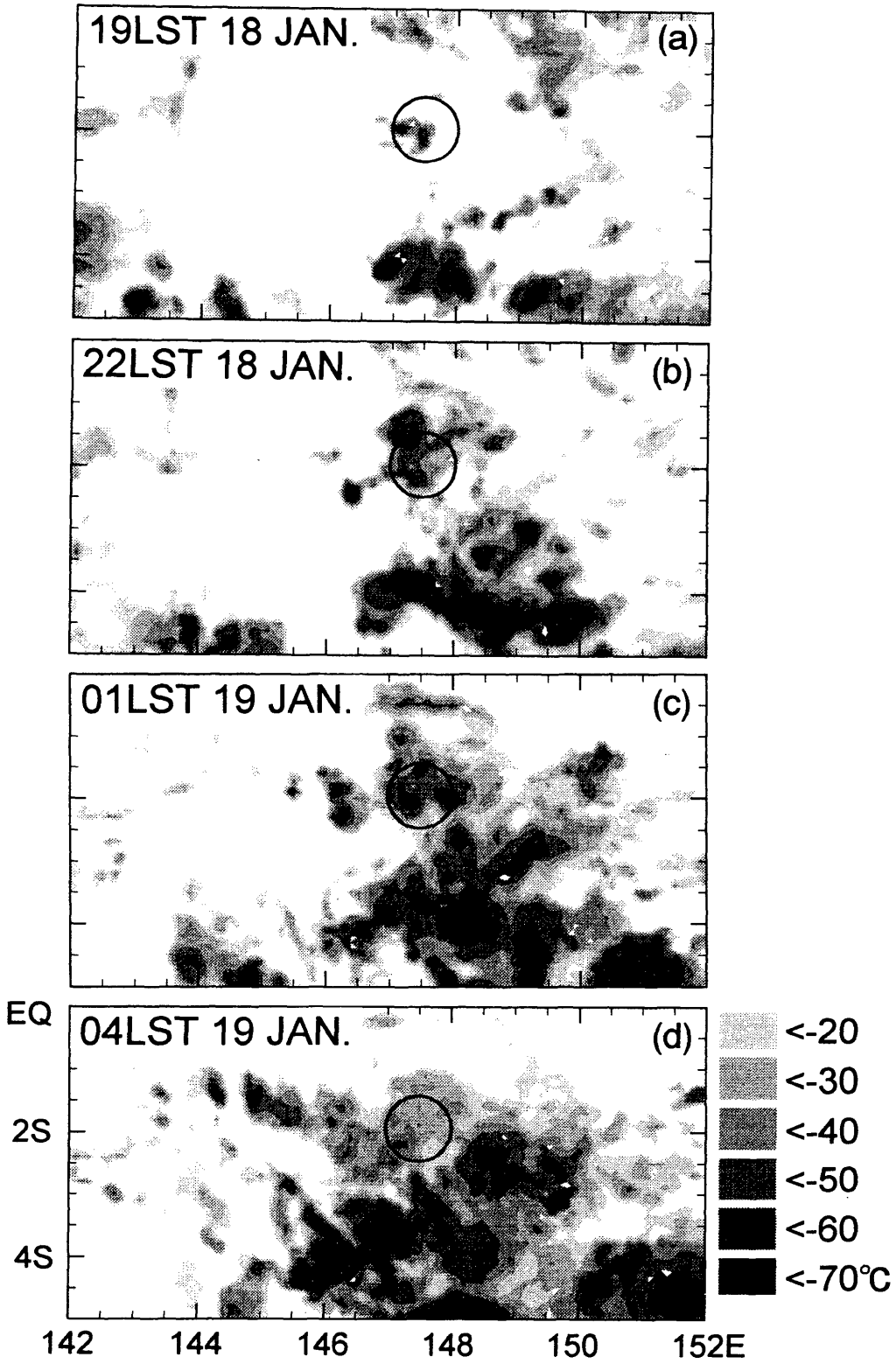

Fig. 3. A sequence of T_{BB} distributions around Manus Island from 1900 LST on 18 to 0400 LST on 19. The circles indicate the range of ILTS radar on Manus Island.

Meteorological Laboratory (HUML). They were installed on Manus Island, Papua New Guinea, which is at the western edge of the outer sounding array of TOGA-COARE. The locations of these radars as well as the information about these radars are described in Uyeda *et al.* (1995).

Three-dimensional data of reflectivity and Doppler velocity were obtained from synchronized vol-

ume scans with elevation angles ranging from 1° to 42° for the HUML-radar, and to 60° for the ILTS-radar. Although one sequence of the volume scans took about 10 minutes, the time interval of the dual-Doppler analysis was 15 minutes because other types of scans were used in addition to the volume scan. These data were interpolated to a Cartesian grid using the Cressman weighting function (1959), applied to five successive azimuths (< 5°), three successive elevation angles, and an influence globe. Using the interpolated data with the common grid of 1.0 km × 1.0 km × 0.5 km from two radars, the horizontal wind field was calculated by a standard dual-Doppler analysis (Armijo, 1969; Ray *et al.*, 1980; Satoh and Wakahama, 1991). To determine the vertical wind field, the continuity equation was integrated upward from the lower boundary. The vertical velocity was adjusted to satisfy the boundary conditions ($w = 0$) at the sea surface and the tropopause (Appendix A).

In addition to the wind field, the data from infrared satellite images and sounding observations were also used. For the hourly infrared images, the Geostationary Meteorological Satellite (GMS), with the 0.1° × 0.1° resolution, over the TOGA-COARE region was used. The 6-hourly sounding observations were operated by National Weather Service at Manus Island, Papua New Guinea with the help of NOAA.

3. Environmental conditions

During the period of a few days prior to the cloud cluster event, there was no detectable cloud system around Manus Island on a synoptic scale, suggesting that the inter-seasonal variations studied by Nakazawa (1988) did not influence the development of the cloud cluster of January 18–19.

Figure 1 shows the vertical profiles of potential temperature θ, equivalent potential temperature θe, and saturation equivalent potential temperature θe^* that was derived from soundings launched before and after a series of rainfalls. At 1600 LST (LST = UTC + 10 hour) on January 18, before the rainfall, the θe profile below the height of 5 km illustrates the convective instability. The lifting condensation level (LCL) was at 735 m. Convective available potential energy (CAPE) was as small as 554 m^2 s^{-2}. This CAPE was typical over small islands like Manus, during TOGA-COARE IOP (Ushiyama *et al.*, 1995). At 0400 LST on January 19, after the rainfall, the θe profile illustrates near neutral stability since the upper layer above the height of 4 km became moist. Near zero CAPE at 0400 LST indicates that the cloud system released the buoyancy energy.

Figure 2 is a wind hodograph before the cloud cluster development. Wind speeds in the troposphere were mostly less than 6 m s^{-1}. The maximum wind speed with a sharp increase was observed at a height of 3 km. Three distinct parts of the large vertical shear of the horizontal wind were presented. The first one was in the lower layer (< 3 km) with its direction from north to south. The second vertical shear had the mean direction of SSW-NNE in the layer between 3 km and 8 km and a maximum between 3 km and 4 km (8.2×10^{-3} s^{-1}). The third one was in the upper layer (> 11 km) with the direction of ESE-WNW.

4. Evolution of the cloud cluster and radar echoes

Figure 3 presents a sequence of T_{BB} maps, from GMS infrared images, showing the evolution of a cloud cluster on January 18–19. This cloud cluster was formed within the radar observation range (circle in Fig. 3a) at 1800 LST, and it kept the same position throughout the development. It extended to both northward and eastward directions with a maximum diameter of about 200 km at 0100 LST on January 19 (Fig. 3c). The hourly variation of the cloud area within the radar range (Fig. 4) reveals that the low T_{BB} area (< −40°C) increased from 1800 LST to 0000 LST and decreased after 0000 LST. The high T_{BB} area (> −30°C), corresponding to an altitude of less than about 10 km, had a peak at 0400 LST. At this time, the cloud cluster was in a dissipating stage, as seen from Fig. 3.

Figure 5a shows the time series of the radar echo area at different levels. The echo area at lower levels (< 4 km) reached the peak at 0200 LST with minor peaks at 2100 LST and 2330 LST (see arrows in Fig. 5a). The comparison between the upper layer (> 10 km) and the lower layer (< 4 km) echo areas at 2100 LST and 0200 LST shows a time lag, approximate 30 minutes per 2 km in height. This fact suggests that the upper echo descended with a velocity of ~1 m s^{-1}, corresponding to the mean terminal velocity of snow particles. The absence of a lag for the 2330 LST peak may be accounted for the lack of snow particles. Figure 5b shows a time series of the total equivalent rain water content for the radar range, calculated from the radar reflectivity data (See Appendix B for the method of calculation). The water content at lower levels rapidly increased from 0100 LST to 0200 LST with small peaks at 2100 LST and 2330 LST. Note the corresponding peaks in echo areas (Fig. 5a). However, the increase in the water content for the 0200 LST peak cannot be explained only by the corresponding peak in the echo area. This suggests that the rainfall rate around 0200 LST was higher than other periods before 0000 LST. Further, it is of particular interest that this increase in the water content occurred only below the melting level (5 km).

Figure 6 shows the hourly Constant Altitude Plan

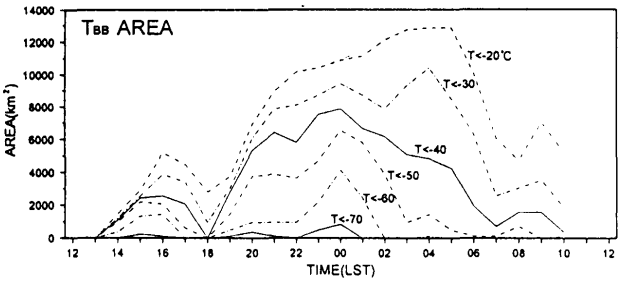

Fig. 4. Time series of the cloud area (T_{BB} < −20°C, ..., < −70°C) within the ILTS radar range derived from the GMS data.

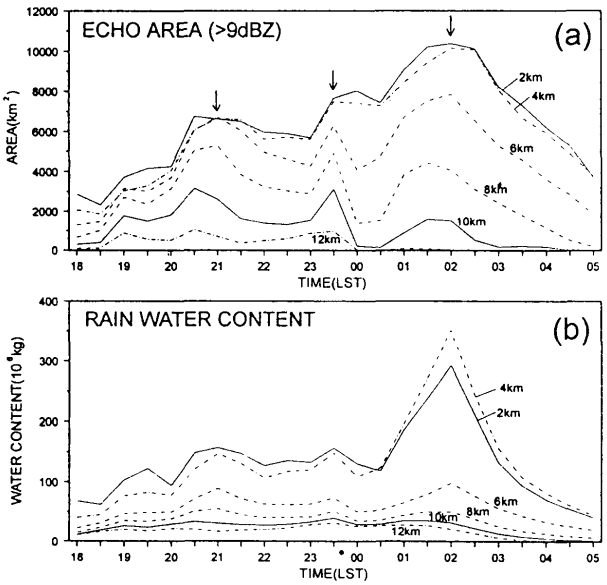

Fig. 5. Time series of (a) the radar echo area (> 9 dBZ) and (b) the equivalent rain water content integrated within the radar range at different levels (2, 4, ..., 12 km). This water content values are obtained from radar reflectivity.

Position Indicator (CAPPI) of radar reflectivity at a height of 2.0 km from 1800 LST on 18 to 0300 LST on 19 January. Although the radar range covered a part of the cloud cluster (see Fig. 3), some characteristic MCSs were observed. Before 0000 LST, some MCSs with a line-shaped echo, composed of convective cells, dominated over the region. At 1900 LST, a characteristic MCS extending from NNE to SSW with a length of ~100 km was observed. According to the sequential CAPPI with 15 minutes intervals, this MCS appeared from 1830 LST to 2100 LST. The orientation of the MCS was almost parallel to the direction of the vertical shear in the lower layer (< 3 km). The mean velocity of convective cells was $u = -0.6$ m s^{-1}, $v = -5.1$ m s^{-1}, which were close to the environmental wind velocity at a height of 3 km (see Fig. 2). The MCS is classified into the slow-moving type, according to the criterion by Barnes and Sieckman (1984), and this MCS is referred to as the slow-moving convective system (SMCS) hereafter.

In contrast, an arc-shaped MCS formed in the north-eastern quadrant at 2000 LST (Fig. 6) moved south-westward with higher speed ($u = -4.5$ m s^{-1}, $v = -7.8$ m s^{-1}) than the SMCS as shown in Fig. 2. This particular MCS was referred to as the fast-moving convective system (FMCS) hereafter. The FMCS was oriented with a large angle to the vertical shear direction in the lower layer. The FMCS was ~60 km in length and ~15 km in width. The FMCS appeared at 1930 LST, and its orientation changed from NNW-SSE to NW-SE caused by the merger between the FMCS and SMCS at around 2000 LST. The FMCS disappeared within the radar range by 2100 LST. In the above description, the vertical shear from the surface to the height of 3 km was compared with the orientation of both the FMCS and the SMCS. Barnes and Sieckman (1984) argued that the vertical shear from the surface to the height of 4 km played an important rôle in determining the orientation of MCSs. However, due to the complexity of MCSs, this characteristic height may vary depending on the vertical scale and exact composition of each MCS. In the present case, the vertical shear direction in the middle layer (3–8 km) may play an important rôle in determining the orientation of the MCS.

After 0000 LST, general echo patterns changed from a convective to a stratiform type. A high-reflectivity region around the radar site (the center of the figures) at 0000 and 0100 LST moved slowly south-westward. A high-reflectivity region rapidly developed between 0100 LST and 0200 LST (see Fig. 5b). It became a wide system with a kink in the northern part. As for the reflectivity pattern, however, hardly any convective cells were found in the region.

5. Kinematic structure of mesoscale convective systems

a. Fast-moving convective system

The fast-moving convective system (FMCS) invaded from the north-eastern part of the radar range at 1900 LST (see Fig. 6). Figure 7 shows the time variation of the horizontal cross section at the height of 3 km. The arc-shaped FMCS propagated south-westward with a velocity of ~9 m s^{-1}, which was faster than the environmental wind velocity (see Fig. 2). The mean orientation of the FMCS was nearly perpendicular to the vertical shear from the height of 3 km to 8 km. The large reflectivity gradient on the west side of the echo system at 1945 LST seemed

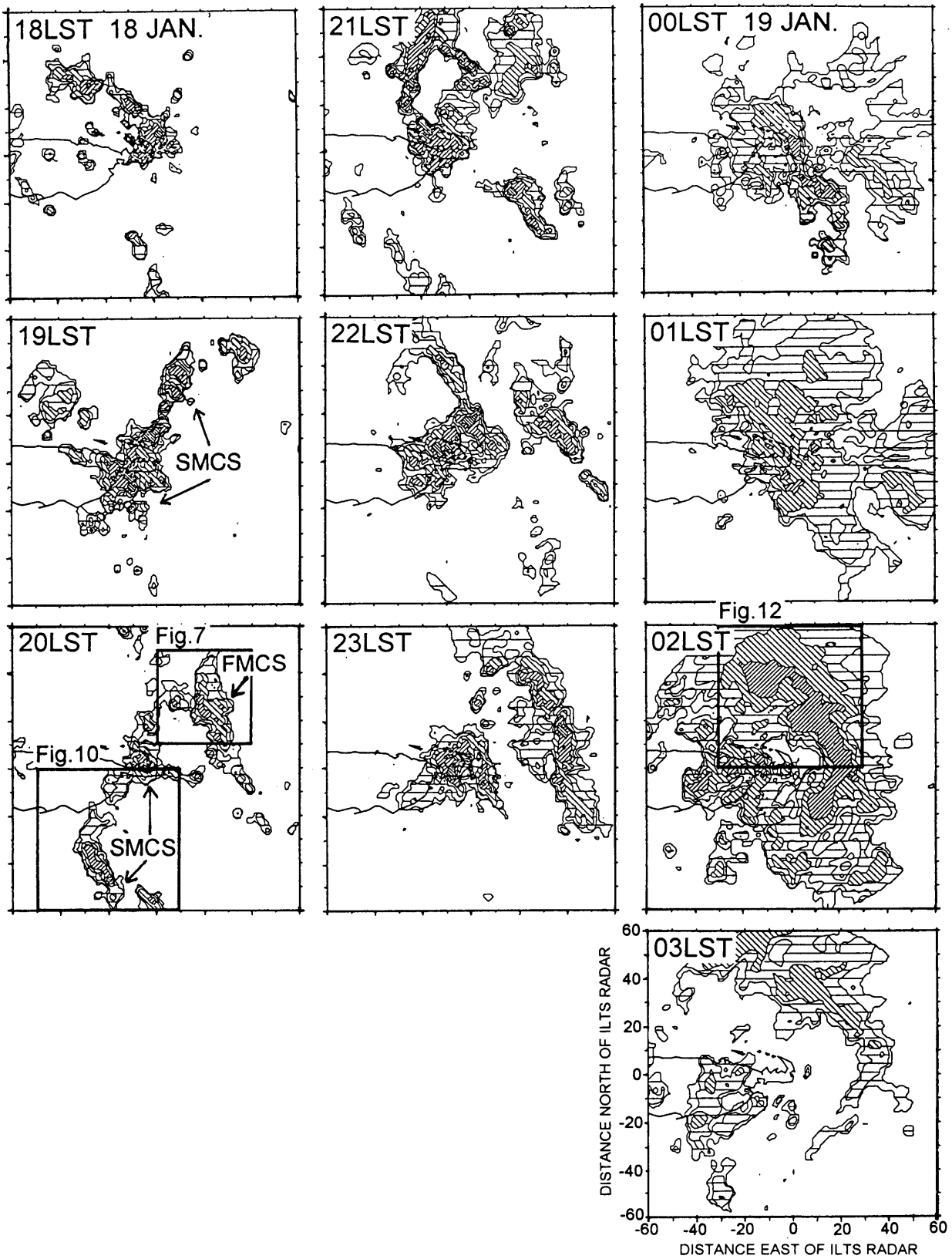

Fig. 6. Sequential horizontal cross sections of radar reflectivity at the height of 2 km derived every 1 hour from ILTS radar. The reflectivity contour interval is 5 dBZ beginning at 15 dBZ. Rectangles at 2000 LST on 18 and at 0200 LST on 19 denote the area of dual-Doppler analysis in Fig. 7, 10, 12.

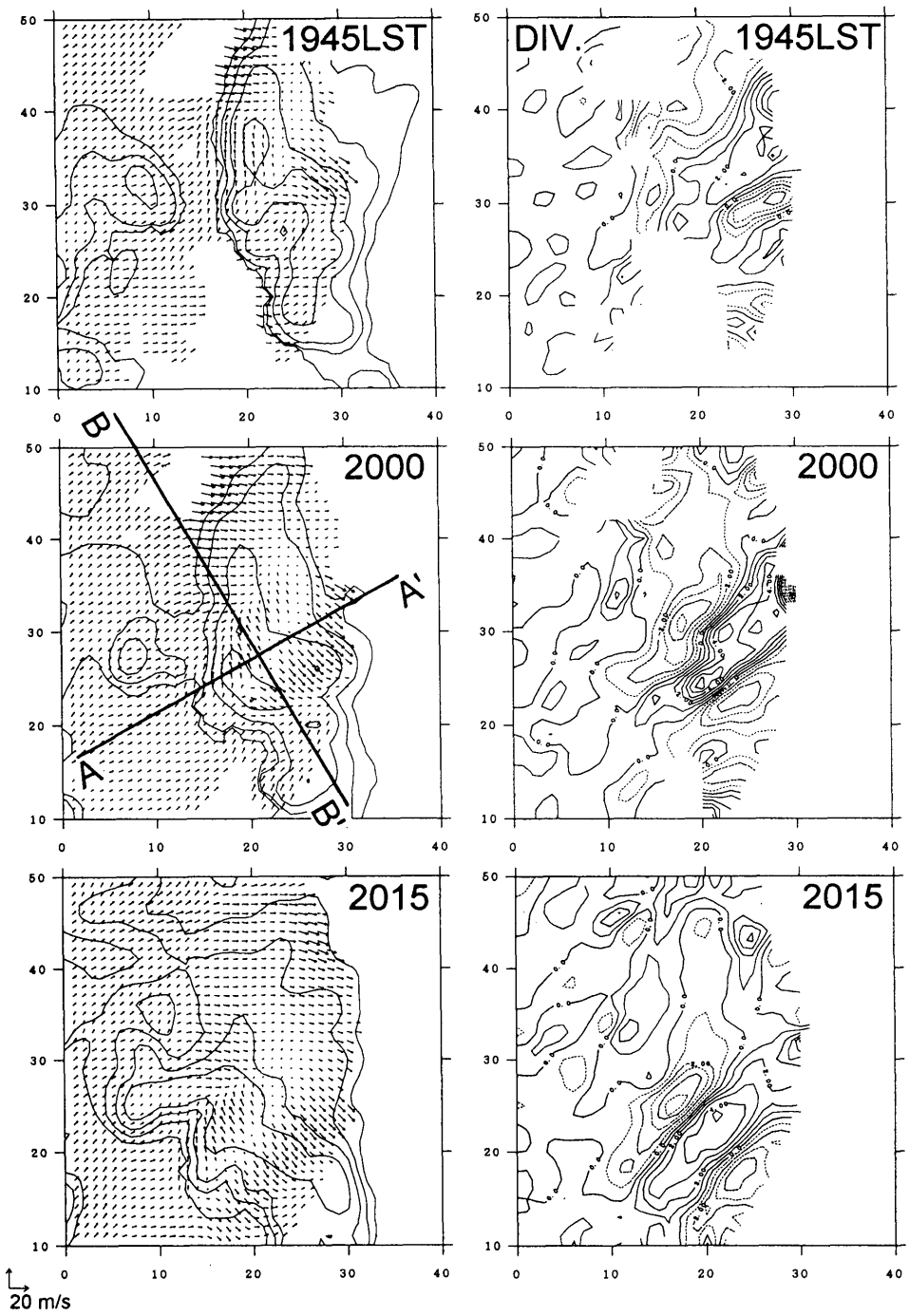

Fig. 7. Horizontal cross sections of the FMCS at 1945, 2000 and 2015 LST at the height of 3 km. In the left panels, storm-relative winds are superimposed on reflectivity contours (every 5 dB beginning at 15 dBZ). In the right panels, divergence contours are shown. The divergence contour interval is 2×10^{-3} s^{-1} with negative value dashed.

to indicate a leading edge. At 2000 LST, however, this reflectivity gradient became smaller. At 2015 LST, the echo shape changed due to a merger with another echo.

The storm-relative wind fields deduced from the dual-Doppler analysis indicate the south-westerly inflow at a height of 3 km. It must be noted that the inflow had two branches in front of a high-reflectivity cell at 2000 LST (near the cross point of line A-A′ and B-B′ in Fig. 7). Behind the cell, southward and northward outflow also appeared. The branching inflow and outflow resulted in a symmetrical distribution of convergence (right panel in Fig. 7). Between the two symmetrical convergence regions, the

divergence region (from $X = 20$ km, $Y = 25$ km to $X = 27$ km, $Y = 32$ km at 2000 LST) extended behind the high-reflectivity cell. The branching of the inflow may be explained by the flow that tries to avoid an obstacle from a strong downdraft. The branching inflow and the distribution pattern of divergence and convergence regions were present at all levels below the height of 4 km. At the height of 3 km (Fig. 7), the convergence was strongest. Above the height of 6 km, the reverse pattern of the divergence and convergence regions was present (not shown here). In spite of the change in echo shape, these distribution patterns were maintained at least between 1945 LST and 2015 LST, suggesting a strong three-dimensional structure.

Figure 8 shows the vertical cross section along line A-A′ in Fig. 7. A storm-relative inflow (distance between 10 km and 25 km) was uniform vertically, contrasting the presence of the vertical shear in the environmental wind field. This suggests that other convective systems, which were lying to the west of the FMCS, modified the wind field. In this cross section, an updraft region appeared over the high-reflectivity cell (distance 29 km). Behind the cell, an older decaying cell was found at 34 km. Furthermore, there was an extension of a weak reflectivity region (between 36 km and 50 km). At upper levels, the upper inflow merged with the updraft, and penetrated into the rear section of the system. The extension of a low-reflectivity region was like an anvil cloud, and resulted from the transportation of ice particles generated in the convective cell by this penetration. This cross section looks similar to one for the squall line (Zipser, 1977), with the difference that this FMCS lacks 'rear inflow' from the low-reflectivity region to the high-reflectivity cell.

Figure 9 shows the sequence of vertical cross sections parallel to the orientation of the FMCS. These cross sections were a composite of the band of 5 km, giving the structure behind the convective cell. The cutting line (B-B′) at 2000 LST was shown in Fig. 7. The horizontal axes of these sections were moved to the left at 5 km per 15 minutes, corresponding to the storm motion. In all cross sections, the vertical shear of horizontal wind was found around the height of 4 km. The significant updrafts appeared above 3 km (distance −12 km at 1945 LST, −8 km and −18 km at 2000 LST, −14 km at 2015 LST), while downdrafts in these sections did not reach the surface. This suggests that convection occurs above the 3 km height, due to the strong convergence between the branching inflow and the outflow (Fig. 7). At 1945 LST, however, a part of the downdraft reached near the surface, and made a gust flow below the height of 1 km at between −15 km and 0 km. It seems that this gust produced the new echo around 5 km at 2015 LST. The first strong updraft (−12 km at 1945 LST) was accelerated between 1945 and 2000 LST. In the period between 2000 and 2015 LST, another updraft was formed and accelerated with a strong echo around −15 km at 2015 LST. By then, the first updraft (−8 km at 2000 LST) was decelerated. It seems that the second updraft was generated by the downdraft (−12 km at 2000 LST) from the first updraft.

At 2000 LST, four updraft regions in the upper level appeared at −8, −18, −28, and −36 km. These updrafts are associated with weak echo regions of less than 10 dBZ. It should be noted that the four pairs of updrafts and weak echo regions had an almost equal interval of about 10 km, suggesting the presence of a gravity wave excited by strong updrafts.

b. Slow-moving convective system

As described in Section 4, the slow-moving convective system (SMCS) was formed at 1830 LST, and maintained its general character for more than two hours. In the first stage of the history, the northern part of the system first developed before 1900 LST, followed by the development in the southern part (2000 LST in Fig. 6). Although convective cells of the SMCS moved southward at a speed of 5 m s^{-1}, the system remained almost stationary in its position.

Figure 10 shows the horizontal section of the southern part of the SMCS at 1945 LST. The cell-relative wind at the height of 2 km was generally weak, but there was a south-easterly inflow on the east side of the SMCS. The vertical velocity distribution at the height of 4 km revealed some individual convective cells. At this stage, most of the cells were still developing, there being only a few downdraft regions. Figure 11 shows the vertical cross sections along lines C-C′ and D-D′ in Fig. 10. The east to west cross section (C-C′) cut through one of identified cells. A dominant easterly flow as a part of the south-easterly inflow and weak westerly inflow converged at the lowest level, generating an updraft around −27 km. The updraft was accelerated below a height of 6 km, becaming an eastward outflow above this height. The another cross section from north to south (D-D′) revealed the southerly inflow as a part of south-easterly inflow at lower levels. This lower inflow formed the dominant updraft over a high-reflectivity cell at 33 km. On the both sides of the high-reflectivity cell, there were two weak cells at 40 km and 26 km. One of them was developing with a separate updraft at 40 km, contrasting another decaying cell. The existence of the three convective cells in different stages of growth suggests that these cells develop alternately. Furthermore, the developing cell on the south indicates that the southerly inflow forms a new convection. Therefore, it seems that the south-easterly inflow plays a most important róle in the development of the SMCS.

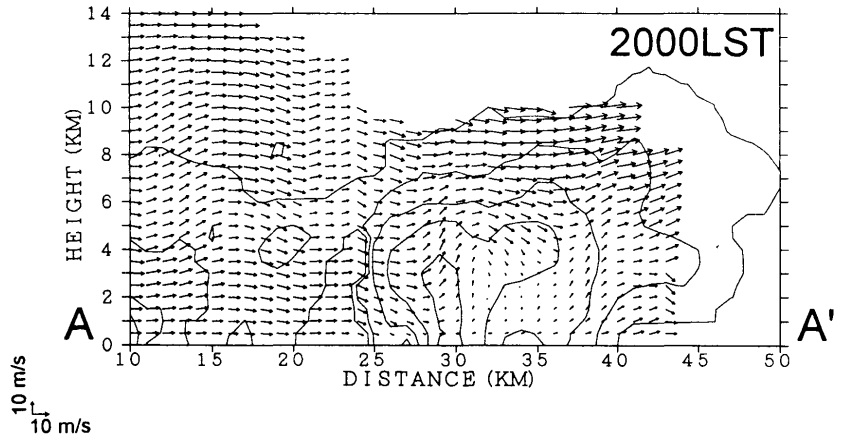

Fig. 8. Vertical cross section cross to the FMCS orientation at 2000 LST. Storm-relative winds are superimposed on reflectivity contours (every 5 dB beginning at 10 dBZ). Location of this section is indicated by line A-A′ in Fig. 7.

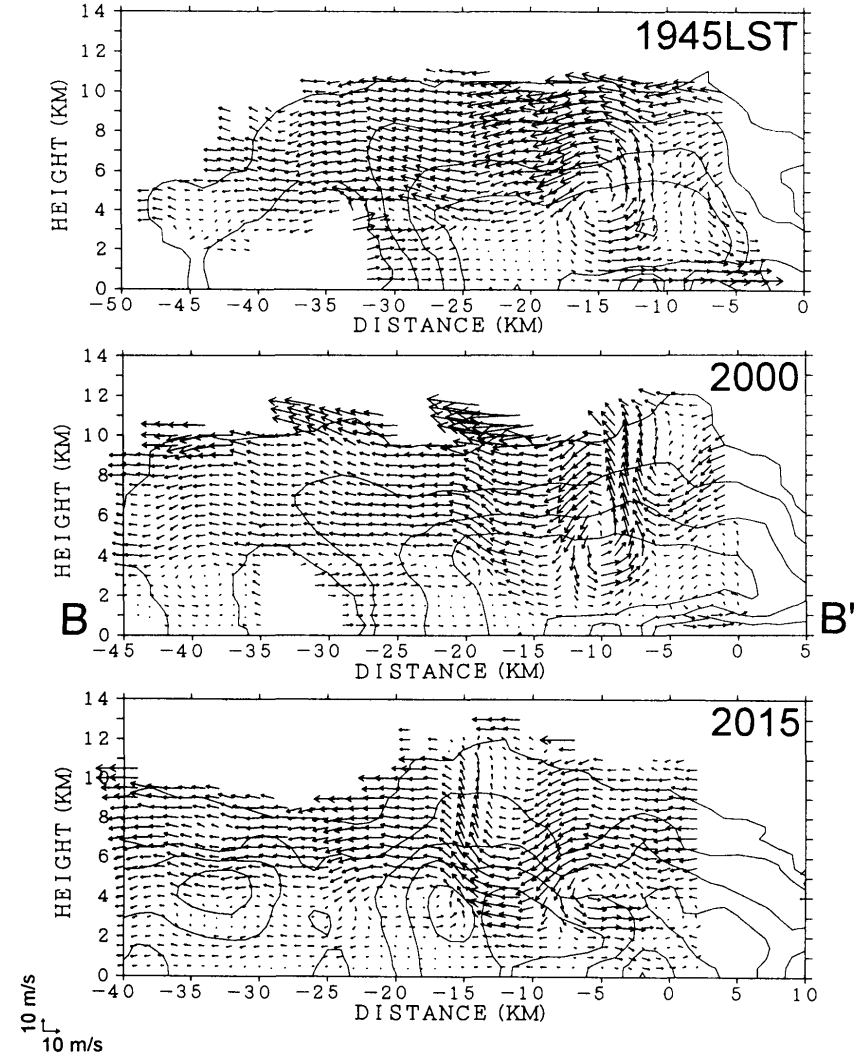

Fig. 9. Composite vertical cross sections along the FMCS orientation at 1945, 2000 and 2015 LST. Storm-relative wind fields are superimposed on reflectivity contours (every 5 dB beginning at 10 dBZ). Location of these sections are indicated by line B-B′ in Fig. 7. These sections are averaged within the band of 5 km cross to these sections. Horizontal coordinates at 2000 and 2015 LST are moved to the left at 5 km per 15 minutes, corresponding to the system motion.

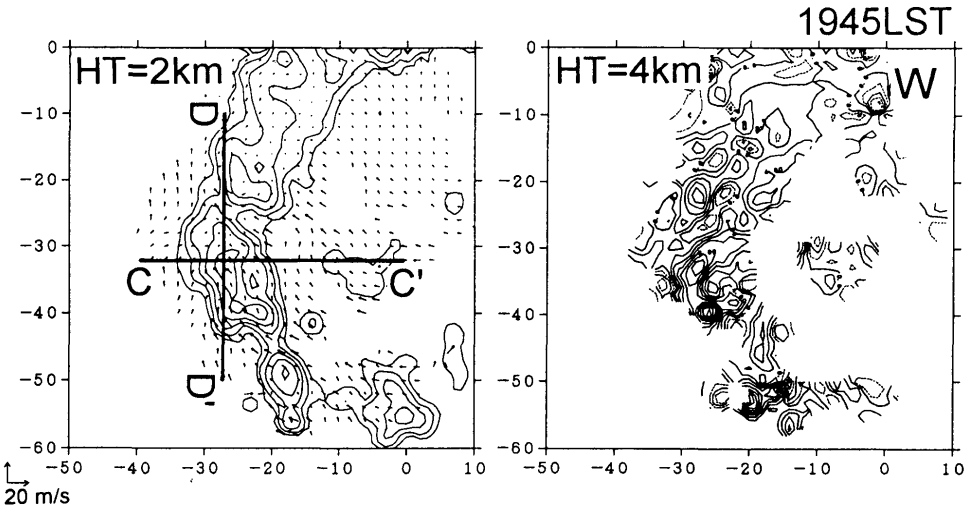

Fig. 10. Horizontal cross sections of the SMCS at 1945 LST. In the left panel, storm-relative wind fields are superimposed on reflectivity contours (every 5 dB beginning at 15 dBZ) at the height of 2 km. In the right panel, vertical velocity contours are shown at the height of 4 km. The interval of vertical velocity contours is 2 m s^{-1} with negative values dashed.

c. Stratiform-looking echo system

There was a maximum in the extent of the stratiform-looking echo at 0200 LST, corresponding the rapid increase in the rain water content at lower levels (Fig. 5). Figure 12 shows the horizontal sections of ground-relative wind fields and reflectivity for the 3, 5 and 8 km heights at 0200 LST. At a height of 3 km, there was a high-reflectivity region with a kink from northwest to southeast. A general divergence field was formed by the southward and westward outflows from the high-reflectivity region. At a height of 5 km, there was a counter-clockwise vortex with its diameter of about 20 km near the center of this section (X = 0 km, Y = 35 km). This vortex extended only between 4 km and 6 km in height. The kink of the high-reflectivity region at the height of 3 km corresponded to the vortex of the middle layer. At a height of 8 km, weak winds prevailed over the entire region. The both updraft and downdraft velocity generally increased up to 8 km with height (right panels in Fig. 12).

A vertical cross section along line E-E′ (Fig. 13) is parallel to the vertical shear direction of a layer between 3 km and 8 km. A clear shear line appeared at the 4 km level over the domain except the northeast region (E′ side). In a layer between 4 km and 6 km, two circulations appeared around 10 km and 23 km. These circulations corresponded to the melting layer indicated by a bright band at a height of 4–5 km. Above 6 km, some circulation could be also found. The downdrafts (distance 13 km and 26 km) of the upper circulations were connected to the middle level circulations. This suggests that the upper level (> 6 km) circulations interacted with the middle level (4–6 km) circulation. In another cross section along line F-F′ (Fig. 13), there were clear upper level circulations. The maximum velocities of the updrafts and downdraft exceeded 5 m s^{-1}. The strong south-easterly flow between −11 km and −27 km at a height of 5 km was a part of the vortex. Below the melting layer, there were only downdraft regions without an updraft region.

It is evident that strong vertical circulations at the middle and upper layer existed within the stratiform-looking echo system. These vertical circulations may be related to the strong vertical shear between 3 km and 4 km, and a release of the latent heat above the melting layer. It seems that the heavy precipitation was caused by these circulations at middle and upper levels, corresponding to the rapid increase of the rain water content in the echo system (Fig. 5).

6. Discussion

A few characteristics of the FMCS are summarized below: (1) The propagation speed (9 m s^{-1}) was faster than the environmental wind velocity. (2) The orientation was nearly perpendicular to the direction of the dominant vertical shear. (3) The arc-shape echo system was approximately 60 km in length and 15 km in width. (4) Behind the high-reflectivity cell, the anvil echo extended to the upper layer. (5) The front inflow branched into two sub-flows in front of the high-reflectivity cell with a strong downdraft. (6) The lower level outflow, caused by the downdraft, extended in both southward and northward directions. The summaries between (1) and (4) suggest that the FMCS would be categorized as squall line, although the horizontal scale was small. In addition, the summaries

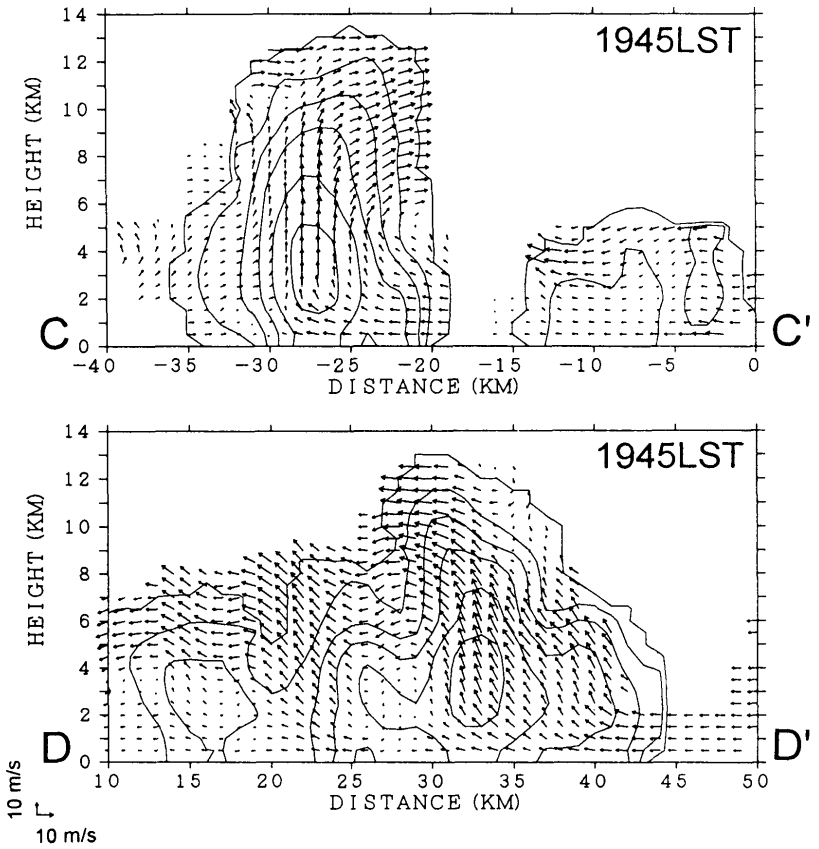

Fig. 11. Vertical cross sections of the SMCS at 1945 LST. Cell-relative wind fields are superimposed on reflectivity contours (every 5 dB beginning at 10 dBZ). Locations of these sections are indicated by the lines C-C′ (west-east) and D-D′ (north-south) in Fig. 10.

of (5) and (6) suggest that the system was similar to a structure produced by the storm splitting shown by Klemp and Wilhelmson (1978). They simulated the evolution of both a right-moving and left-moving storm in the constant shear environment using a three-dimensional cloud model. Rotunno (1981) gave the explanation that the storm splitting was caused by the presence of both positive and negative vorticity from the tilting of a vortex tube of the vertical shear in a convection. From the strong vertical shear between 3 km and 4 km, it seems that this mechanism is also applicable to the present case. The first updraft in the south-east part developed at 1945 LST, while the another cell in the north-west part developed at 2015 LST, thus giving a time delay of about 30 minutes (see Fig. 9). Hence, the evolution of the FMCS is different from that of the storm splitting, that does not have such a time delay in general, even though the structure of the FMCS is similar to the one with the storm splitting. One of the possible mechanisms to explain this delay is that downdrafts generated by the first convection triggered off the second convection. Another mechanism may be that the upper flow transported ice particles north-westward (the left side in Fig. 9), evidenced by the ESE to WNW direction of the environmental wind in the upper layer. The presence of thunder and lightning, observed by a radar operator, and the above analysis suggest the vigorous convection with a three-dimensional structure like a supercell.

As described before, the FMCS and the SMCS are classified as squall line and non-squall line, respectively. It is interesting that the two types of MCSs coexisted (2000 LST, Fig. 6). A similar case was reported by House (1977), Mansfield (1977) and Ogura and Liou (1980), although squall and non-squall lines are associated with different environment conditions (Barnes and Sieckman, 1984). It is of concern that the structure of MCSs may be not decided uniquely by the environmental conditions (Ogura, 1990).

To understand the kinematic difference among the three echo systems, the vertical velocity fields and the divergence were averaged over three areas corresponding to the FMCS, the SMCS and the stratiform-looking echo system (Fig. 14).

First, we describe the difference between the FMCS and the SMCS. For the FMCS, the strongest updraft exceeding 25 m s^{-1} was observed near the

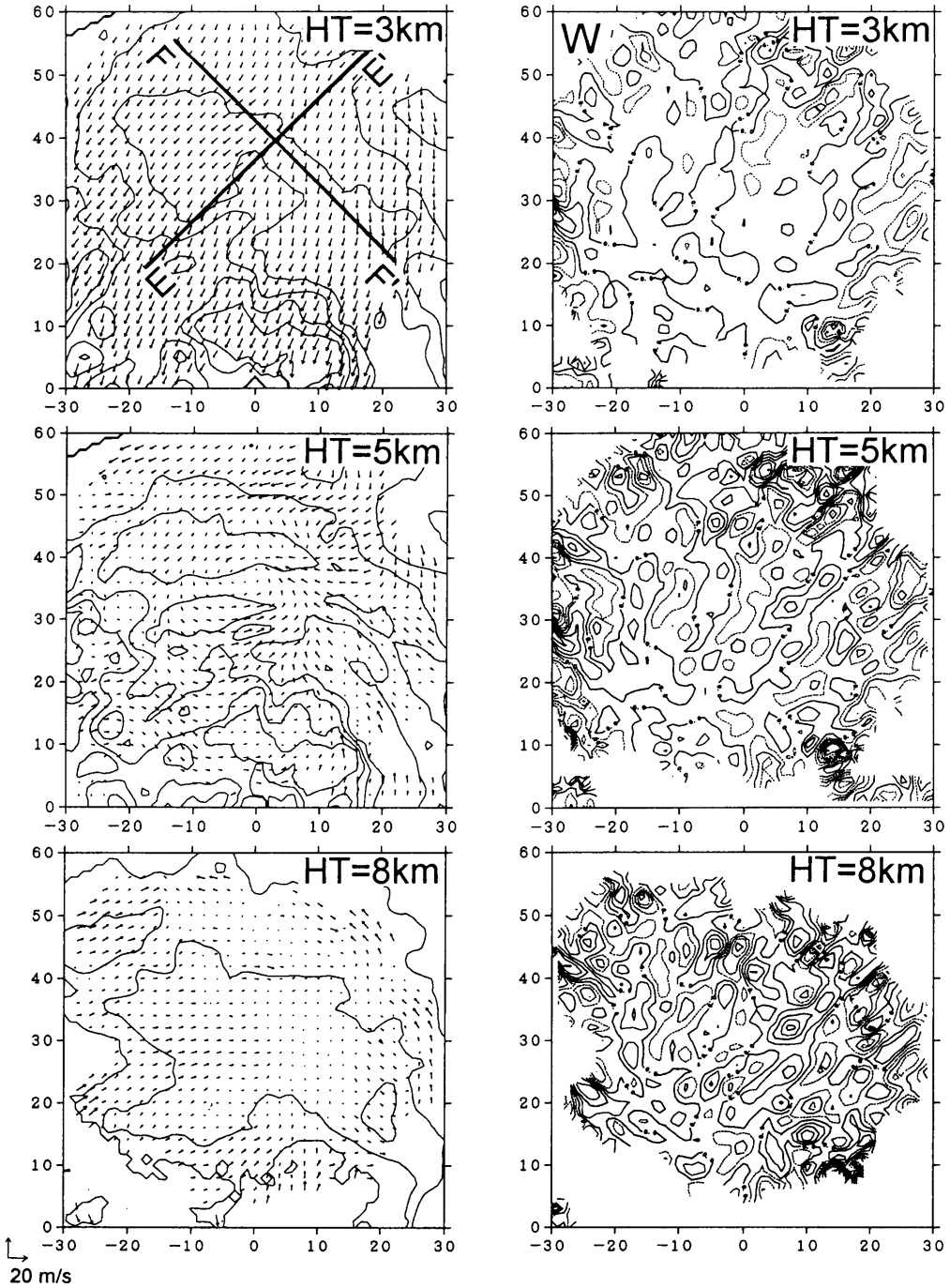

Fig. 12. Horizontal cross sections of the stratiform-looking echo system at the height of 3 km, 5 km and 8 km at 0200 LST. In the left panels, ground-relative wind fields with superimposed reflectivity contours (every 5 dB beginning at 15 dBZ) are shown. In the right panels, vertical velocity contours are shown. The interval of vertical velocity contours is 2 m s^{-1} with negative values dashed.

7 km level, and the updraft and the maximum downdraft with a peak near 5 km were similar in their magnitude (Fig. 14a). For the SMCS, the magnitude of the updraft was close to the FMCS updraft. However, the maximum downdraft of the SMCS was smaller than that of the FMCS at almost all levels. The area-averaged vertical velocity for the SMCS was upward at all levels below 12 km, and was larger than that of the FMCS (Fig. 14b). The area-averaged convergence at lower levels and the divergence at upper levels for the SMCS were also larger than these for the FMCS (Fig. 14c). These suggest that the dominant developing cells with updraft existed in the SMCS. For both FMCS and SMCS, maximum updrafts exceeded 20 m s^{-1}, though the CAPE was only 554 m^2 s^{-2}. This discrepancy may

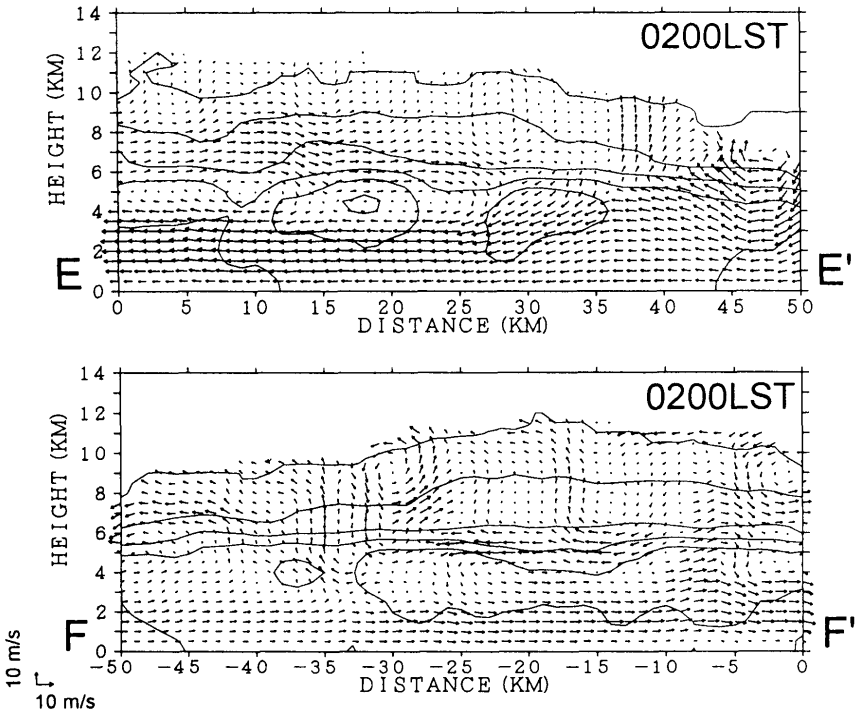

Fig. 13. Vertical cross sections of the stratiform-looking echo system at 0200 LST. Ground-relative wind fields with superimposed reflectivity contours (every 5 dB beginning at 10 dBZ) are shown. Locations of these sections are indicated by line E-E′ and F-F′ in Fig. 12.

be due to small convections around Manus Island at 1600 LST with which the sounding became biased (see Fig. 4). Another possible reason is that some MCSs, which develop and decay repeatedly, change the basic environment conditions.

Secondly, the double peaks in the area-averaged vertical velocity for the FMCS and the SMCS were described (Fig. 14b). The lower peaks were found at around 5 km, and the upper peaks were appeared at about 10 km. Observing their height, it is probable that the lower peaks were associated with the release of latent heat around the melting level. The gravity waves excited by the strong convection seem to cause the upper peaks, with the areal difference between updraft and downdraft regions. The reason for the few downdraft areas compared with the updraft areas in the upper layer, is that ice particles with radar detectable sizes are fewer in the downdraft regions due to the evaporation of the particles. Heymsfield *et al.* (1991) found strong downdrafts associated with convectively gravity waves by aircraft investigation. In the present case, Fig. 9 shows indirect evidence for the gravity waves, which was excited by the strong updraft in the FMCS.

Finally, we describe the stratiform-looking echo system. The maximum vertical velocity increased above the height of 4 km (Fig. 14a), corresponding to the vertical circulations in the middle and upper layers presented in Section 5c. Figure 14a shows that the vertical circulation in the upper layer had a strong updraft and downdraft whose maximum velocity reached 5 m s^{-1}. On the other hand, the area-averaged vertical velocity in the stratiform-looking echo system exhibited an obvious downdraft at about 4 km height (Fig. 14b). The enhanced downdraft around the melting level was explained by a melting cooling (Leary and Houze, 1979b). At the upper levels, the area-averaged divergence was either negative or near zero. In contrast, the area-averaged divergence below 4 km was positive. These features are similar to ones suggested by Biggerstaff and Houze (1993) for a 'secondary band' behind a squall line. The area-averaged vertical velocity at the upper levels was near zero, though the strong updraft or downdraft appeared above the melting level (Fig. 14a), indicating the balance in the mass fluxes of updraft and downdraft above the melting level.

7. Concluding remarks

Three distinct mesoscale convective systems, composing a tropical cloud cluster, observed on January 18–19, 1993 were investigated by the dual-Doppler radar analysis. The cloud cluster was formed within the radar range with a diameter of about 200 km in the matured stage. The environmental wind was weak, but a strong vertical shear existed in the middle layer. The maximum extent in high T_{BB}

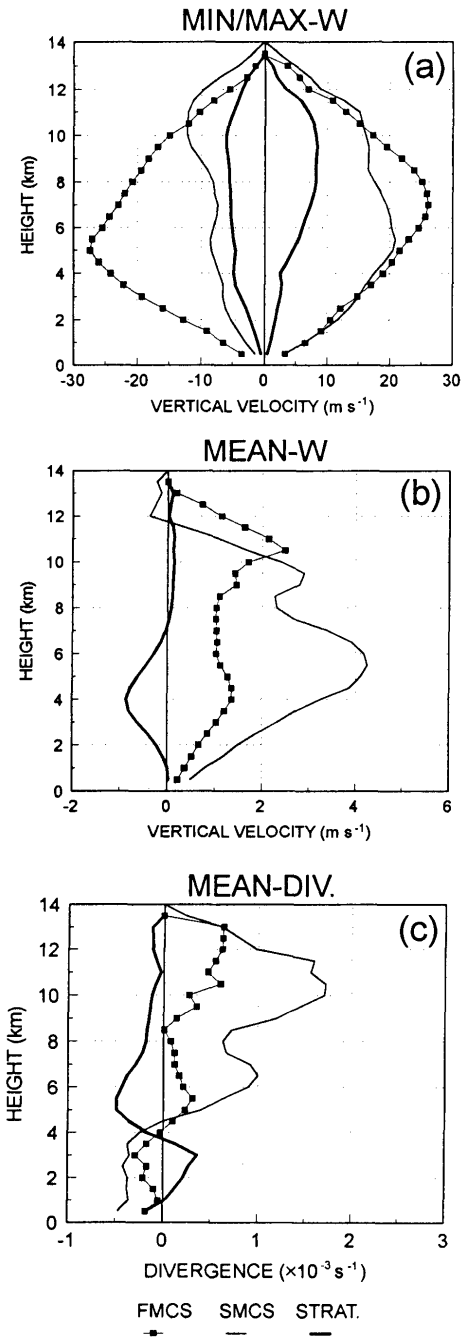

Fig. 14. Vertical profile of (a) minimum and maximum vertical velocity, (b) area-averaged vertical velocity and (c) area-averaged divergence. Thin lines with small square denote the FMCS, thin lines denote the SMCS and thick lines denote the stratiform-looking echo system. Area-averaged ranges in the FMCS, the SMCS and the stratiform-looking echo are 10 km $< X <$ 30 km and 10 km $< Y <$ 50 km (20 LST), -35 km$< X <$20 km and -45 km $< Y <$ 25 km (20 LST), -10 km $< X <$ 10 km and 20 km $< Y <$ 40 km (02 LST), respectively.

($>$ 30°C) and low T_{BB} ($<$ -40°C) areas had a 4-hours delay. The maximum extent of the lower echo area also had a lag of 30 minutes per 2 km in height, corresponding to the mean fall velocity of snow particles. The total rain water content and the echo area in the lower layer reached their maximum at 0200 LST on 19. At this time, the stratiform-looking echo was dominant over the radar range. During the period from 0100 to 0200 LST, the water content increased rapidly with the rate higher than that of echo area extension.

The cloud cluster was composed of some mesoscale convective systems (MCSs). In the first stage, convective echo regions dominated over the radar range, while in the latter stage, the stratiform-looking echo system became more dominant.

One of characteristic MCSs (FMCS) propagated south-westward at a speed of 9 m s^{-1}, which was faster than the environmental wind velocity. The FMCS was about 60 km in length and 15 km in width, and its orientation was nearly perpendicular to the direction of the dominant vertical shear. Behind the convective cell, the anvil echo extended to upper levels. These results suggest the characteristic of this FMCS is similar to that of a squall line, except of a smaller size. The internal structure revealed by a dual-Doppler analysis had a three-dimensional air flow. The front inflow branched into two sub-flows in front of a strong downdraft region. The lower level outflow from the downdraft extended in both southward and northward directions. The branching inflow and the two outflows made symmetrically arranged strong convergence regions at lower levels. The maximum updraft velocity at the convergence region was higher than 25 m s^{-1}. These kinematic structures were similar to the structure produced by the storm splitting shown by Klemp and Wilhelmson (1987).

Another characteristic MCS (SMCS) was composed of individual convective cells, which moved slowly with an environmental wind near the height of 3 km. Since the SMCS extended in a line parallel to the vertical shear direction, the system almost kept its position. This SMCS was triggered by the south-easterly inflow at lower levels. At upper levels, an anvil echo extended to the down-shear direction with the dissipation of the convective cell in the middle layer.

The stratiform-looking echo system appeared in the latter stage of the cloud cluster. In this system, a vortex with a diameter of about 20 km was found between 4 km and 6 km levels. In the middle layer (4–6 km), some vertical circulations were found. In the upper layer ($>$ 6 km), some strong circulations with the maximum vertical velocity of 5 m s^{-1} were also found. These results suggested that the stratiform-looking echo system with an obvious bright band was convective above the middle

layer. The rain water content increased rapidly in the system as a result of heavy precipitation produced by these circulations in the middle and upper layers.

Acknowledgments

The authors wish to thank Prof. K. Takeuchi of Hokkaido University and Dr. Y. Fujiyoshi of Nagoya University for their valuable comments and encouragement. The authors are grateful to the members of Doppler radar observation group in Manus and National Weather Service of Papua New Guinea for their support in our observation. Special thanks are due to Mr. M. Ohi of ILTS and crew members of Kaiyo and Natsushima of JAMSTEC for the radar installation and transport. Thanks are extended Dr. M. Yoshizaki, Mr. S. Nakai and anonymous reviewer for their useful comments. Thanks are also extended to Mr. T. Ushiyama and Mr. D. Abe of ILTS for supporting this study. The GMS data were provided by Dr. T. Nakazawa of MRI, JMA.

The numerical calculations were carried out on a HITAC, S-820 in the Calculation Center of Hokkaido University. This research was supported by Grant-in-Aid for Creative Basic Research (J-COARE) and for JSPS Fellows from the Ministry of Education, Science and Culture.

Appendix

A. Adjustment method of the vertical velocity in the dual-Doppler analysis.

In the dual-Doppler analysis, it is difficult to determine the boundary conditions of w. Unfortunately, some Doppler radar data do not extend to the surface due to ground clutter contamination. Furthermore, a convective echo top height is different from a cloud top when the convective echo does not reach the tropopause so that the boundary condition ($w = 0$) at the echo top height can not be adopted.

Ray *et al.* (1980) introduced an adjustment method of u, v, and w using a variational integral constraint to satisfy the continuity equation under the given lower and upper boundary conditions. In this paper, however, simpler method, in which only the vertical velocity field is adjusted, was used. First, the vertical velocity is calculated by a relaxation method using the upward integration of the continuity equation from the surface boundary condition of $w = 0$. Next, the vertical velocity in the no-echo region above the echo top is estimated, assuming that the divergence is constant, equivalent to the constant vertical gradient of w above the echo top level. After the vertical velocity is filled up to the tropopause, the adjusted w at level z^l is written

$$w^l = w_0^l + \frac{z^l}{z^T}(w^T - w_0^T), \quad w^T = 0, \tag{1}$$

where w^T is the boundary condition of the tropopause, the subscript 0 denotes an observed value, and the superscript l indicates a level. When the echo regions do not reach the surface, the adjusted w after the lower region filled up by a similar argument is written

$$w^l = w_0^l + \frac{z^T - z^l}{z^T}(w^S - w_0^S), \quad w^S = 0, \tag{2}$$

where w^S is the surface boundary condition. This equation is an effective application of a downward integration of the continuity equation. In present case study, however, the upward integration was adopted because there were more errors in estimating vertical velocity for the upper levels than for the lower levels. Using both Equations (1) and (2), it is possible to adjust the vertical velocity in a region lacking both upper and lower data. Finally, the vertical velocity in the no-echo regions are eliminated, because the assumption of the constant divergence above the echo top is not applicable when the cloud top does not reach the tropopause.

B. Calculation of the equivalent rain water content.

The equivalent rain water content can be calculated from radar reflectivity using the Z-R relationship and mean fall velocity of particles (Fujiyoshi *et al.* 1992). Since the Z-R relationship of ILTS-radar in the tropical precipitation have not been investigated, we adopted the general relationship by Marshall and Palmer (1948),

$$Z = 200R^{1.6} \tag{3}$$

where Z (mm^6 m^{-3}) is an equivalent reflectivity factor and R (mm hr^{-1}) is a rainfall rate. The mean terminal velocity Vt (m s^{-1}) is obtained from the following equation by Rogers (1964),

$$Vt = 3.8Z^{1/14} \tag{4}$$

Using Equations (3) and (4), the equivalent rain water content M (g m^{-3}) is calculated from

$$M = 1000R/3600Vt. \tag{5}$$

R and Vt calculated from Ze are averaged over each grid (1 km × 1km × 0.5 km) so that the total rain water integrated M_{total} (g) is given by,

$$M_{total} = 5 \times 10^8 \sum_{i=1}^{n} M_i \tag{6}$$

where n denotes the all grids in a layer.

References

Akaeda, K., T. Yokoyama, A. Tabata, M. Ishihara and H. Sakakibara, 1991: Evolution of the kinematic structure within a meso-β-scale convective system in the growing and mature stages. *Mon. Wea. Rev.*, **119**, 2664–2676.

Armijo, L., 1969: A theory for the determination of wind and precipitation velocities with Doppler radars. *J. Atmos. Sci.*, **26**, 570–573.

Barnes, G.M. and K. Sieckman, 1984: The environment of fast- and slow-moving tropical mesoscale convective cloud lines. *Mon. Wea. Rev.*, **112**, 1782–1794.

Biggerstaff, M.I. and R.A. Houze, Jr., 1993: Kinematics and microphysics of the transition zone of the 10–11 June 1985 squall line. *J. Atmos. Sci.*, **50**, 3091–3110.

Chen, Y.L., 1985: Tropical squall lines over the eastern Atlantic during GATE. *Mon. Wea. Rev.*, **113**, 2015–2022.

Chong, M., P. Amayenc, G. Scialom and J. Testude, 1987: A tropical squall line observed during the COPT 81 experiment in West Africa. Part I: Kinematic structure inferred from dual-Doppler radar data. *Mon. Wea. Rev.*, **115**, 670–694.

Cressman, G.W., 1959: An operational objective analysis system. Mon. Wea. Rev., 87, 367–374.

Fujiyoshi, Y., K. Tsuboki, S. Satoh and G. Wakahama, 1992: Three-dimensional radar echo structure of a snow band formed on the lee side of a mountain. *J. Meteor. Soc. Japan*, **70**, 11–24.

Houze, R.A., Jr., 1977: Structure and dynamics of a tropical squall-line system. *Mon. Wea. Rev.*, **105**, 1540–1567.

Houze, R.A., Jr. and A.K. Betts, 1981: Convection in GATE. *Rev. Geophys Space Phys.*, **19**, 541–576.

Heymsfiels, A.J., R. Fulton and J.D. Spinhirne, 1991: Aircraft overflight measurements of Midwest severe storms: Implications of geosynchronous satellite interpretations. *Mon. Wea. Rev.*, **119**, 436–456.

Ishihara, M., 1985: Statistical analysis of radar echoes observed in the equatorial western pacific during summer MONEX in 1979. *J. Meteor. Soc. Japan*, **63**, 210–225.

Keenan, T.D. and S.A. Rutledge, 1993: Mesoscale characteristic of monsoonal convection and associated stratiform precipitation. *Mon. Wea. Rev.*, **121**, 352–374.

Klemp, J.B. and R. Wilhelmson, 1978: Simulations of right- and left-moving storms through storm splitting. *J. Atmos. Sci.*, **35**, 1097–1110.

Leary, C.A. and R.A. Houze, Jr., 1979a: The structure and evolution of convection in a tropical cloud cluster. *J. Atmos. Sci.*, **36**, 437–457.

Leary, C.A. and R.A. Houze, Jr., 1979b: Melting and evaporation of hydrometers in precipitation from the anvil clouds of deep tropical convection. *J. Atmos. Sci.*, **36**, 669–679.

Marshall, J.S. and W.M. Palmer, 1948: The distribution of raindrops with size. *J. Meteor.*, **5**, 16–18.

Mansfield, D.A., 1977: Squall lines observed during GATE. *Quart. J. Roy. Meteor. Soc.*, **103**, 569–574.

Mori, K., 1992: Internal structure and time evolution of a cloud cluster in the western tropical pacific region observed by Keifu Maru. *J. Meteor. Soc. Japan*, **70**, 1111–1123.

Nakazawa, T., 1988: Tropical super clusters within interseasonal variations over the western Pacific. *J. Meteor. Soc. Japan*, **66**, 823–839.

Ogura, Y. and M.T. Liou, 1980: The structure of a midlatitude squall line. *J. Atmos. Sci.*, **37**, 553–567.

Ogura, Y., 1990: Effect of environment on the structure and organization of mesoscale convective systems. *Tenki*, **37**, 439–465 (in Japanese).

Ray, P.S., C.L. Ziegler, W.C. Bumgarner and R.J. Serafin, 1980: Single and multiple Doppler radar observations of tornadic storms. *Mon. Wea. Rev.*, **108**, 1607–1625.

Rogers, R.R., 1964: An extension of the Z-R relation for Doppler radar. *Proc. 11th Weath. Radar Conf.*, 158–161.

Rotunno, R., 1981: On the evolution of thunderstorm rotation. *Mon. Wea. Rev.*, **109**, 557–586.

Roux, F., 1988: The west African squall line observed on 23 June 1981 during COPT 81: kinematics and thermodynamics of the convective region. *J. Atmos. Sci.*, **45**, 406–426.

Satoh S. and G. Wakahama, 1991: Dual-Doppler radar measurements of a three-dimensional kinematic wind field. *Low Temp. Sci.*, **50**, 23–35 (in Japanese with English summary).

Smull, B.F. and R.A. Houze, Jr., 1987: Dual-Doppler radar analysis of a midlatitude squall line with a trailing region of stratiform rain. *J. Atmos. Sci.*, **44**, 2128–2148.

Ushiyama, T., S. Satoh and K. Takeuchi, 1995: Time and spatial variations of mesoscale rainfalls and their relation to the large-scale field in the western tropical Pacific. *J. Meteor. Soc. Japan.*, **73**, 379–392.

Uyeda, H., Y. Asuma, N. Takahashi, S. Shimizu, O. Kikuchi, A. Kinoshita, S. Matsuoka, M. Katsumata, K. Takeuchi, T. Endoh, M. Ohi, S. Satoh, Y. Tachibana, T. Ushiyama, Y. Fujiyoshi, R. Shirooka, N. Nishi, T. Tomita, H. Ueda, T. Sueda and A. Sumi, 1995: Doppler radar observations on the structure and characteristics of tropical clouds during the TOGA-COARE IOP in Manus, Papua New Guinea — Outline of the observation —. *J. Meteor. Soc. Japan.*, **73**, 415–426.

Zipser, E.J., 1977: Mesoscale and convective-scale downdrafts as distinct components of squall-line structure. *Mon. Wea. Rev.*, **105**, 1568–1589.

TOGA-COARE 集中観測期間中のパプアニューギニア、マヌス島における雲群の構造に関するドップラーレーダー観測：2台のドップラーレーダーによる雲群を構成するメソ対流系の解析

佐藤晋介
(北海道大学低温科学研究所)
木下　温[1]・上田　博
(北海道大学理学部地球物理学科)

1993年1月18–19日に観測されたクラウドクラスターと、それを構成する3つの特徴的なメソ対流系を2台のドップラーレーダーデータを用いて解析した。2台のレーダーは、TOGA-COARE集中観測期間中にマヌス島 (南緯2°、東経147°) に設置したものである。解析したクラウドクラスターは、レーダー観測範囲内で発生し直径約200 kmにまで発達した。この時の環境の風は弱かったが、高度3~4 kmに強い鉛直シアーが存在した。

このクラウドクラスターは幾つかのメソ対流系によって構成されており、クラスターの成長期には対流性エコーが、衰退期には層状性エコーが卓越していた。最初の特徴的なメソ対流系 (FMCS) は環境の風より速い速度で伝播し、その走向は鉛直シアーの方向にほぼ直交していた。また、強い対流セルの後方には層状性エコーが広がっていた。FMCSに流入する流れは強い下降流を伴うセルの前で2本に分かれ、その下降流から南と北方向に発散する下層の流れとの間に対称性を持つ2つの強い収束域を形成した。これらの特徴から、FMCSは'storm splitting'が作り出すような3次元気流構造を持つスコールラインとして認識された。2番目のメソ対流系 (SMCS) は、ゆっくりとした移動速度を持つ独立した対流セルで構成され、系全体の走向は鉛直シアーに平行であった。3番目のシステムは、明瞭なブライトバンドを伴う層状性エコーであったが、その中層 (高度4~6 km) には直径約20 kmの水平渦が見つかった。さらに、中層と上層 (高度6 km以上) には5 m s^{-1}に達するような鉛直速度を持つ鉛直循環が見つかり、これらによって多量の降水が生成されたことが分かった。

[1]現所属：別海高校、北海道